Civil Engineering Infrastructures Journal xx,xx

DOI: 10.22059/ceij.2025.401578.2379

Assessment of Opening Dimensions on Internal Pressure Coefficients in Barrel Vault Roofs

Khosravi, H.[1,*], Bahram, M.[2], and Esmaily, A.[3]

[1]Assistant Professor, Department of Civil Engineering, Hakim Sabzevari University, Sabzevar, Iran; Corresponding Author: h.khosravi@hsu.ac.ir

[2]Department of Civil Engineering, Hakim Sabzevari University, Sabzevar, Iran; E-mail: mohammadbahram438@gmail.com

[3]Department of Civil Engineering, Hakim Sabzevari University, Sabzevar, Iran; E-mail: alizadehtb@gmail.com

Received: 31/08/2025

Revised: 04/10/2025

Accepted: 29/11/2025

A B S T R A C T

Accurate estimation of wind loads on barrel vault structures is essential for achieving reliable and economical design. Due to their curved geometry and the sensitivity of wind load distribution to structural form, the prediction of aerodynamic behavior in these roofs remains challenging, particularly when large openings are present. This study focuses on quantifying the influence of opening dimensions on the internal wind pressure patterns of barrel vault roofs. A total of 49 numerical models with various opening ratios and height-to-span configurations were analyzed under Terrain Category C conditions, with wind speed and turbulence intensity defined according to ASCE 7. The findings indicate that both the absolute size of openings and the windward-to-leeward opening ratio significantly modify internal pressure coefficients,

leading to changes in net wind forces on the structure. The analysis revealed that barrel vaults with a height-to-span ratio of 0.1 provided the most uniform internal pressure distribution. When inlet and outlet openings are balanced, the internal pressure coefficient (Cp) ranges between -0.1 and 0.1 for opening ratios from 0.1 to 0.5, whereas unbalanced openings result in full-surface suction or pressure, providing practical guidance for optimizing barrel vault roof designs. The novelty of this work lies in providing a systematic parametric assessment of opening geometry effects on barrel vaults, offering practical insights for code development and safe design of large-span roof systems. The numerical simulations were performed using widely accepted computational methods, ensuring consistency with established practices.

Alternative keywords: Barrel vault structures, CFD simulation, Wind pressure, Structural openings

1. **Introduction**

The barrel vault, as a widely used structural form for covering large-span areas without intermediate columns, plays a significant role in modern construction—particularly in industrial facilities, stadiums, terminals, and similar structures. In order to achieve an optimal design, structural engineers must not only consider aesthetic aspects but also account for the influence of form on the load-bearing capacity under both gravity and lateral loads, considering the geographical location of the structure.

Although barrel vaults are generally stable under symmetric loads, they are vulnerable to asymmetric loads such as wind and snow, with reported cases of structural failure (Mahdi,

2004). Accurate and economical design requires reliable data on wind load distribution on both external and internal surfaces. Existing codes often lack detailed guidance for curved structures, especially those with large openings, which can significantly influence wind forces. This study investigates the effect of opening dimensions on the wind load distribution of barrel vault structures. In the first part, the pressure coefficient distribution on the external surface of barrel vaults with different height-to-span ratios is examined. In the second part, the influence of openings on internal pressure distribution is analyzed. For this purpose, the optimal height-to-span ratio is selected, and the internal pressure coefficient is evaluated for inlet and outlet openings with different area ratios. In total, 49 models with various opening configurations are simulated and analyzed.

Over the years, numerous studies have been conducted—using both wind tunnel testing and numerical simulations—on boundary layer flow over curved structures. These have focused on factors such as surface roughness, Reynolds number, and upstream terrain irregularities. However, none of these studies has specifically addressed the influence of opening dimensions in barrel vault structures.

This aspect is critical because multiple variables can affect wind force magnitude, and understanding the behavior of boundary layer flow in response to different opening sizes can provide engineers with valuable insights for optimal design. Therefore, this research focuses on the impact of opening dimensions in barrel vault structures under wind loads. Previous studies have examined the effect of wind load on double-arched domes with varying arch

heights. Khosrowjerdi et al. conducted numerical simulations to analyze the wind pressure coefficient (Cp) at various points on domes with fixed height-to-span ratios situated on Type C ground. Their numerical results were validated against experimental data. The findings demonstrated that factors such as arch height, location, and connection area of the two arches significantly influence the distribution of wind pressure (Khosrowjerdi and Sarkardeh, 2022).

Letchford and Sarkar (2000) studied the effect of surface smoothness and roughness on parabolic domes, examining a dome with a height-to-span ratio of 0.31 under open terrain category C conditions using wind tunnel tests (ASCE, 1998). **Cheng and Fu (2000)** investigated the influence of Reynolds number on spherical domes under laminar and turbulent flow. **Pratap and Rani** (2025) proposed a new parametric equation to predict wind pressure coefficients on low-rise mono-slope canopy roof buildings. Their study highlighted the influence of roof geometry and wind direction on external pressure distribution, providing useful insights for understanding the effects of wind on complex roof shapes.

Hoor et al. (2003) studied wind pressure distribution on complex dome geometries (circular, parabolic, and traditional Eastern-style domes) using 2D computational wind tunnel simulations with ANSYS. The domes were exposed to a constant 35 m/s wind in a smooth, obstacle-free domain. They presented graphs of pressure, maximum wind speed, and peak suction versus dome height, which served as design pressure curves.

In recent years, studies have focused on wind pressure coefficients on curved roofs with openings. **Cheon et al. (2024)** conducted wind tunnel tests on dome roofs with various

openings and proposed adjusted pressure coefficients for windward areas. **Rani et al. (2024)** analyzed single- and multi-span cylindrical canopy roofs, providing contour maps of net pressure coefficients. **Liu et al. (2024)** performed CFD analyses on renovated historical buildings, highlighting curvature and turbulence effects on internal pressure. **Ding et al. (2024)** used LES and wind tunnel tests on vaulted-free roofing systems, identifying key arcs' response trends. **Pagnini et al. (2022)** measured pressure coefficients on a vaulted canopy roof, reflecting geometry and opening configurations aligned with barrel vault structures.

Sun et al. (2015) conducted experiments to evaluate the effect of Reynolds number variations and roof-dependent parameters on semi-cylindrical roofs under uniform turbulent and laminar wind conditions.

In recent years, the influence of openings on wind pressure distribution in vaulted and curved roof structures has gained significant attention in structural engineering. **Li et al. (2025)** conducted a comprehensive study on an airport terminal roof, showing that open roof conditions can substantially increase negative wind pressures in certain areas, affecting structural stability and safety. This research underscores the importance of accounting for the size and location of openings in wind load analysis and provides a solid foundation for studies on barrel vaults and other curved roofs. **Yao et al**. (2024) used numerical simulations to show that roof geometry, including span-to-rise ratio and cross-section, strongly affects wind pressure coefficients. **Ding** and Uematsu (2022) conducted wind tunnel experiments on vaulted free roofs, measuring both external and internal pressures and proposing design wind force

coefficients. These works highlight the importance of geometry and wind direction on pressure distribution, while the effects of opening dimensions on internal pressures in barrel-vaulted roofs remain underexplored. **Lee** et al. (2022) studied wind pressures on elliptical retractable dome roofs. They showed that the size and position of openings significantly affect internal and external pressure coefficients, highlighting the importance of opening geometry in wind design. **Shukla** (2024) investigated the effect of lateral loads, including wind-induced forces, on the structural performance of high-rise reinforced concrete buildings. The study highlighted the importance of structural layout and placement of shear walls in controlling lateral displacements and stresses. Although the focus was on high-rise buildings rather than vaulted roofs, the findings emphasize how structural geometry and load paths influence wind-induced effects, providing useful insights for understanding the response of complex roof geometries under wind loading.

In the present study, CFD techniques are used to examine how height-to-span ratio and opening dimensions affect wind load distribution in barrel vault structures. **Khosrowjerdi, Sarkardeh, and Kioumarsi (2021)** conducted numerical analyses on heritage domes, showing that architectural features and environmental conditions significantly influence wind pressure distribution and structural response.

Despite numerous studies on wind loads over curved roofs, there is a lack of systematic investigation on how varying opening sizes and their ratios affect internal pressure distributions in barrel vaults.

This study aims to fill this gap by numerically analyzing 49 barrel vault models with different height-to-span ratios and various inlet/outlet opening configurations, providing insights into optimal design for internal pressure distribution under wind loads.

Table 1. Summary of previous studies on wind loads in curved and vaulted roof structures

Author(s), Year	Structure Type	Method	Main Findings	Limitations / Notes
Letchford & Sarkar (2000)	Parabolic dome (h/span = 0.31)	Wind tunnel	Effect of surface roughness and smoothness on wind load distribution	Focus on small dome, limited to external pressure
Cheng & Fu (2000)	Spherical domes	Wind tunnel (laminar & turbulent)	Reynolds number significantly affects aerodynamic characteristics	No openings considered
Pratap & Rani, 2025	Low-rise mono-slope canopy roof building	Parametric equation (numerical/ analytical study)	Proposed a new parametric equation for wind pressure coefficients; highlighted the influence of roof geometry and wind direction on external pressure distribution	Focused on low-rise, single-slope roofs; internal pressures not considered; applicability to complex vaulted roofs needs further study
Hoor et al. (2003)	Circular, parabolic, Eastern domes	CFD (ANSYS)	Dynamic pressure curves provided for different dome geometries	2D models, simplified assumptions
Mahdi (2004)	Barrel vaults	Case studies	Reported structural failures under asymmetric loads (wind, snow)	Descriptive, not quantitative
Sun et al. (2015)	Semi-cylindrical roofs	Wind tunnel	Effect of Reynolds number and roof parameters on pressure distribution	Focused on external loads
Khosrowjerdi & Sarkardeh (2022)	Double-arched domes	Numerical + validation	Arch height & connection area strongly affect pressure distribution	Different geometry from barrel vaults

Author(s), Year	Structure Type	Method	Main Findings	Limitations / Notes
Cheon et al. (2024)	Dome roofs with openings	Wind tunnel	Adjusted Cp values proposed for windward openings	Dome shape, not barrel vault
Rani et al. (2024)	Cylindrical canopy roofs	Wind tunnel	Contour maps of net Cp across spans	Limited span range
Liu et al. (2024)	Curved historical roofs	CFD under typhoon	Curvature and turbulence model affect internal pressures	Case-specific heritage structures
Ding et al. (2023)	Vaulted free roofs	LES + wind tunnel	Identified arc response trends in Cp	General vaulted roofs
Pagnini et al. (2022)	Vaulted canopy roof with openings	Wind tunnel	Pressure coefficients directly affected by opening geometry	Close to barrel vaults but canopy type
Li et al. (2025)	Terminal roof with openings	CFD + experiments	Roof openings increase negative pressure, affect stability	Not focused on barrel vault geometry
Khosrowjerdi et al. (2021)	Heritage domes	Numerical	Architectural details influence Cp distribution	Heritage domes, not barrel vaults

Positioning of the present study:

Unlike previous works, the current research systematically investigates **the effect of opening dimensions and windward-to-leeward opening ratios on internal wind pressure of barrel vault roofs**, filling the gap in literature regarding opening configurations in this specific structural form.

2. Materials and Methods

Fluid dynamics problems are governed by three fundamental conservation laws: the conservation of mass, momentum, and energy. These laws are expressed in the form of partial differential equations, which are discretized for numerical analysis. The conservation of mass, also known as the continuity equation, is given as follows (Horr et al., 2023; Reddy and Gartling et al., 2000):

$$\frac{\partial \rho}{\partial t} + \frac{\partial (\rho U_x)}{\partial x} + \frac{\partial (\rho U_y)}{\partial y} + \frac{\partial (\rho U_z)}{\partial z} = 0 \quad (1)$$

Ux,Uy,Uz are the velocity components in the three coordinate directions x, y, and z, respectively.

Other standard relations such as the equation of state, stress tensor definitions, and Newtonian fluid assumptions are omitted here for brevity and can be found in standard references (e.g., ANSYS Inc., 2017).

Based on these fundamental relations, the governing momentum equation can be written as follows:

$$\frac{\partial \rho U_x}{\partial t} + \frac{\partial (\rho U_x U_x)}{\partial x} + \frac{\partial (\rho U_y U_x)}{\partial y} + \frac{\partial (\rho U_z U_x)}{\partial z} = \rho g_x - \frac{\partial P}{\partial x} + R_x + \frac{\partial}{\partial x}\left(\mu_e \frac{\partial U_x}{\partial x}\right) + \frac{\partial}{\partial y}\left(\mu_e \frac{\partial U_x}{\partial y}\right) + \frac{\partial}{\partial z}\left(\mu_e \frac{\partial U_x}{\partial z}\right) + T_x \quad (2)$$

gx is the component of gravitational acceleration in the x-direction; ρ\rhoρ is the fluid density; μe\mu_eμe is the effective viscosity; Rx is the distributed resistance, and Tx represents energy dissipation due to viscosity. Both Rx and Tx are added by the user to the equations to account for the effects of certain geometric obstacles or viscous effects on the fluid flow without explicitly modeling their geometry.

The non-tensorial form of the above equations can be found in reference (Uematsu et al., 2001).

In this study, ANSYS 18.2 software along with the RANS-RNG turbulence model was used for modeling, and the CFD results were validated using the work of Letchford and Sarkar (2000).

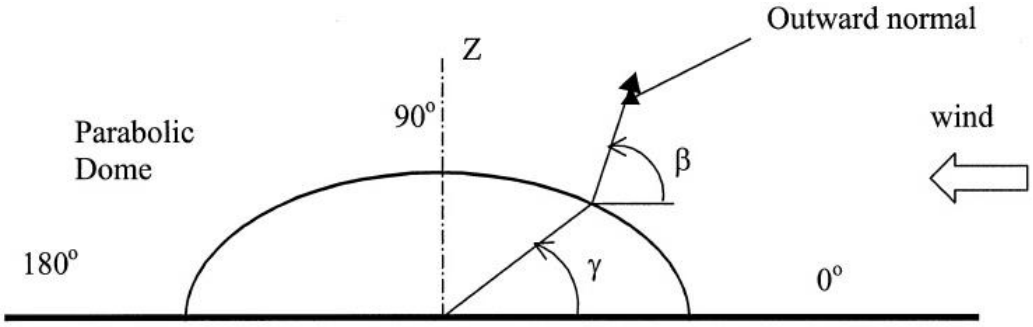

Fig. 1. Dome of the Letchford and Sarkar laboratory model (Letchford and Sarkar, 2000).

In the Letchford and Sarkar laboratory model (Letchford and Sarkar, 2000), the dome base diameter is 0.48 meters, with wind speed and turbulence intensity at the dome apex being 18 m/s and 15%, respectively, scaled at 1:300. This study uses terrain category C according to the ASCE7-98 standard (ASCE, 1998). The average wind velocity profile based on height in the wind tunnel and ASCE7-98 code, as well as the input velocity profile applied in the software, are shown in Figure (2-a). The turbulence intensity profile in the wind tunnel and ASCE7-98, along with the turbulence intensity profile applied in the software, are presented in Figure (2-b). It is worth noting that the software does not allow direct application of the turbulence intensity profile; therefore, turbulence kinetic energy (K) and the turbulence kinetic energy dissipation rate (ε) profiles were used instead. K is obtained from Equation (3), and ε from Equations (4 and 5) (ANSYS, 2017).

$$K = \frac{3}{2}(u_{avg} I)^2 \tag{3}$$

$$\varepsilon = \frac{K^{3/2}}{l} \tag{4}$$

$$l = \frac{0.07L}{C_\mu^{3/4}} \tag{5}$$

where u_{avg} is the average flow velocity, I is the turbulence intensity, L is the dome diameter, and Cμ is the turbulence model constant, which Lander has determined to be 0.09 for this constant (ANSYS, 2017).

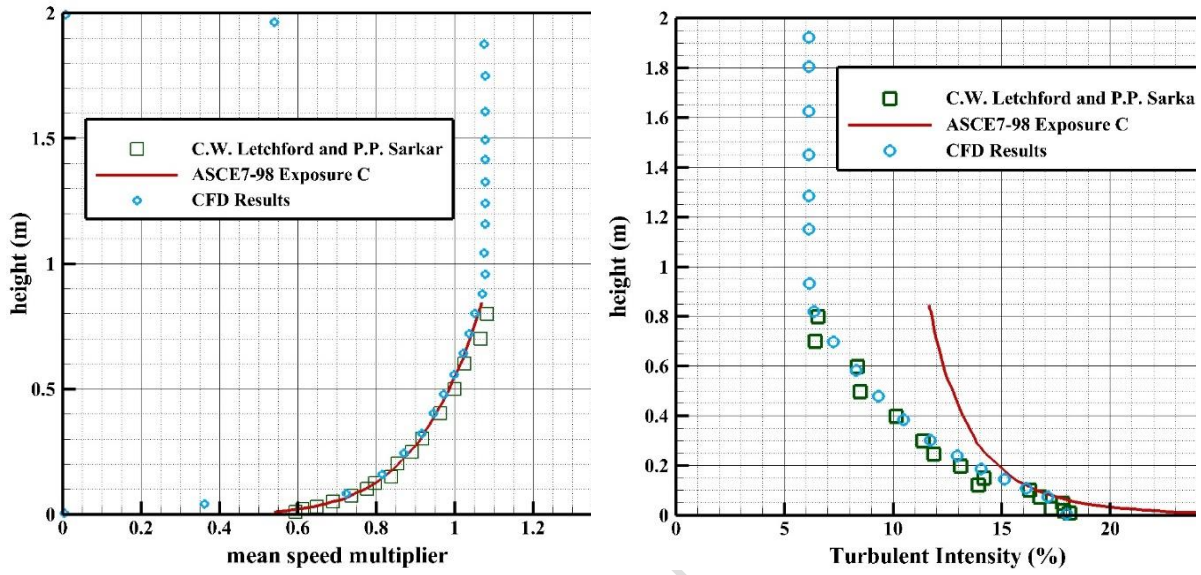

2-b **2-a**

Fig. 2. (2-a) Applied input turbulence intensity profile and (2-b) applied input velocity profile extracted from the numerical model, compared with the input turbulence intensity profile and input velocity profile from the experimental model (Letchford and Sarkar, 2000) and ASCE7-98 code for type C terrain.

One of the key considerations in CFD modeling is selecting an appropriate computational domain to avoid interference from side walls and to ensure proper inlet and outlet boundary conditions. The domain dimensions were set to 2 × 5.2 × 12 meters, ensuring a blockage ratio below 2% (Figure 3).

It is worth noting that since the objective of this research is to investigate the loading condition on curved structures without addressing the structural response to this loading, and also considering that spatial structures (especially domes) widely include single-layer and multi-

layer lattice structures and shell structures—with the common characteristic of high stiffness—this leads to relatively small deformations in such structures.

Moreover, since the fluid pressure distribution on a body depends not only on the velocity and properties of the fluid but also on the shape of the body's surface, these models can be considered as rigid surfaces.

The boundary conditions applied in this simulation are presented in Figure 3.

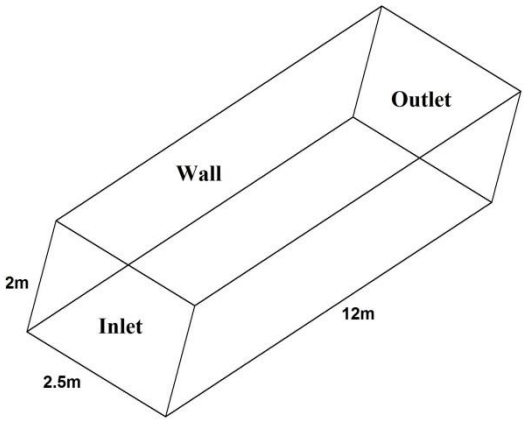

Fig. 3. Computational domain of the numerical flow simulation.

To analyze the sensitivity of the results to mesh size, five different mesh sizes were examined. The Cp diagram corresponding to the numerical simulation of the experimental model (Letchford and Sarkar, 2000) for different mesh sizes is shown in Figure 4-a.

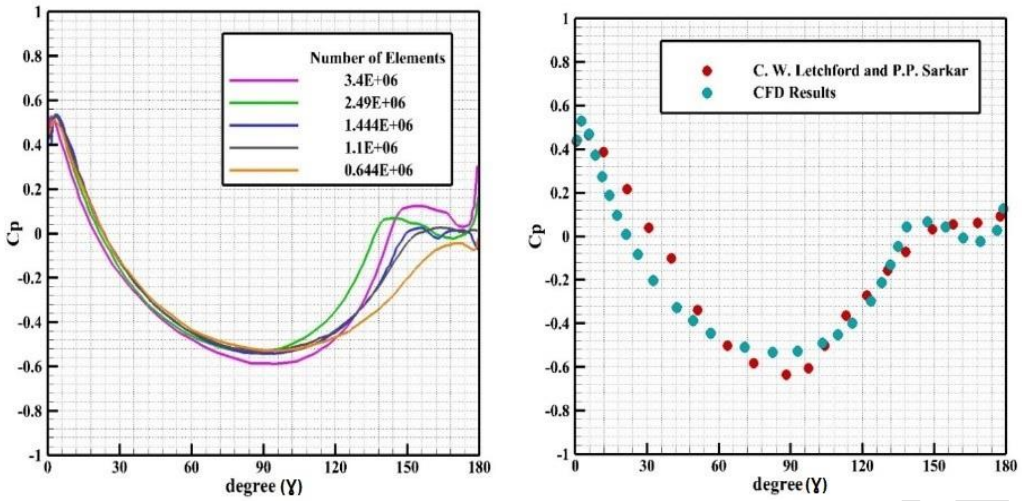

4-b **4-a**

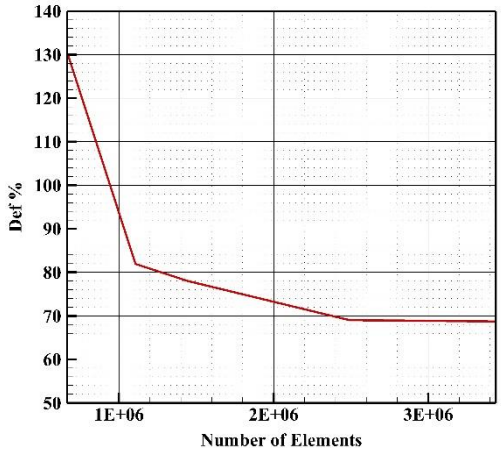

4-c

Fig. 4. Grid independence chart for the numerical simulation of the experimental model (Letchford and Sarkar, 2000)

As shown in Figure 4-a, by comparing the Cp curves obtained from the experimental model with those from numerical models using different mesh sizes, a mesh independence study was conducted, and the mesh that best matched the experimental model was selected. Figure 4-b presents the Cp curves of the experimental model and the numerical model with the selected mesh size. In Figure 4-c, the percentage difference between various mesh sizes in the numerical

model and the experimental results is shown. As observed in Figure 4-c, the mesh with 5.2 × 10^6 elements provides the best agreement with the experimental model (Letchford and Sarkar, 2000).

3. Results and Analysis

This study investigates the effect of opening dimensions in barrel vault structures on the distribution of internal wind pressure coefficients. The flow domain, inlet velocity, turbulence intensity, span diameter, meshing, and other input variables are considered similarly to the parabolic dome simulation described in Section 2, assuming terrain category C according to ASCE 7-98.

In the first part, the distribution of the pressure coefficient on the external surface of barrel vaults with height-to-span ratios of 0.1, 0.2, 0.3, 0.4, 0.5, and 0.6 is examined. Subsequently, in the second part, the effect of openings on the internal pressure coefficient distribution of the barrel vaults is analyzed. For this purpose, the optimal height-to-span ratio of the barrel vault is selected, and the internal pressure coefficient distribution is calculated with opening area ratios (opening area to total smooth surface area) on each side equal to 0.1, 0.2, 0.3, 0.4, 0.5, 0.6, and 1. Consequently, a total of 49 models with various opening ratios in the barrel vault are studied and analyzed.

3.1 Wind Load Distribution on Barrel Vault Structures with Different Height-to-Span Ratios

In this section, the distribution of wind pressure coefficients on barrel vault structures is investigated, focusing on the influence of the height-to-span ratio on the pressure coefficient distribution. After modeling and analyzing the structures using ANSYS Fluent 18.2, pressure coefficient contour maps for the studied barrel vaults are presented in Figures 5 through 10. In these figures, the wind direction is from left to right.

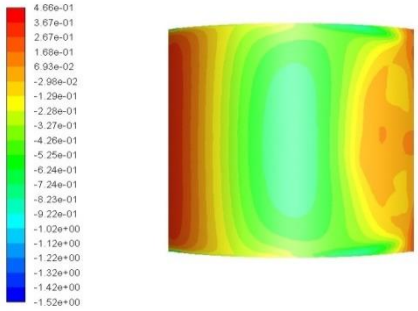

Fig. 6. Contour of pressure coefficient distribution on the barrel vault with a height-to-span ratio of 0.2.

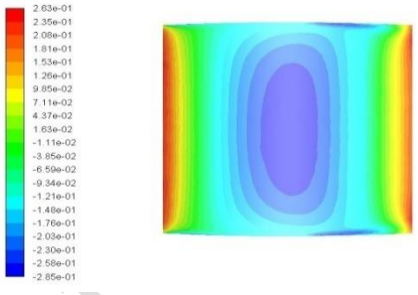

Fig. 5. Contour of pressure coefficient distribution on the barrel vault with a height-to-span ratio of 0.1.

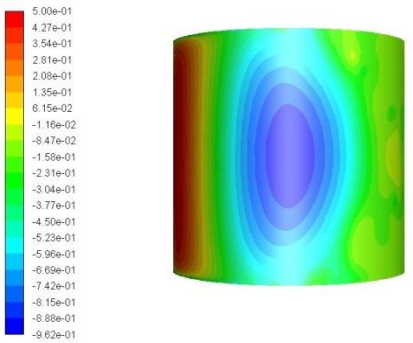

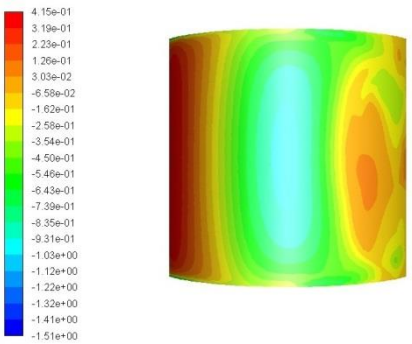

Fig. 8. Contour of pressure coefficient distribution on the barrel vault with a height-to-span ratio of 0.4.

Fig. 7. Contour of pressure coefficient distribution on the barrel vault with a height-to-span ratio of 0.3.

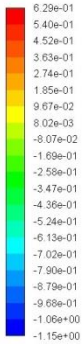

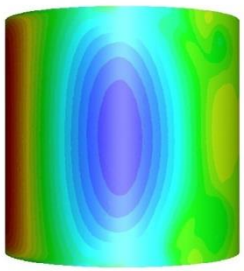

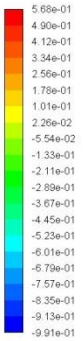

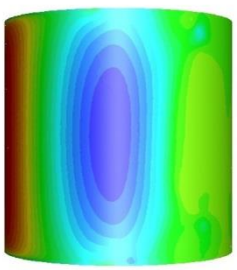

Fig. 10. Contour of pressure coefficient distribution on the barrel vault with a height-to-span ratio of 0.6.

Fig. 9. Contour of pressure coefficient distribution on the barrel vault with a height-to-span ratio of 0.5.

Table 2 summarizes the maximum and minimum internal pressure coefficients (Cp) obtained from Figures 5–10 for vaults with different height-to-span ratios.

Height-to-span ratio (Figure)	Max Cp	Min Cp	Location of Max Cp	Location of Min Cp	Overall regime
0.1 (Fig. 5)	0.263	-0.285	Front	Side edges + center	Mostly pressure with suction zones
0.2 (Fig. 6)	0.466	-1.52	Front	Flat sides, center	Suction except front 1/3
0.3 (Fig. 7)	0.415	-1.51	Front	Flat sides, center	Mixed (small pressure + suction)

0.4 (Fig. 8)	0.500	-0.962	Front	Center	Suction except front 1/3
0.5 (Fig. 9)	0.568	-0.991	Front	Center	Suction except front 1/3
0.6 (Fig. 10)	0.629	-1.15	Front	Center	Suction except front 1/3

Trend Summary for Figures 5 to 10 (Height-to-Span Ratio Study):

- **Maximum Pressure:** Increases as the height-to-span ratio increases, from 0.263 at 0.1 to 0.629 at 0.6. The maximum pressure consistently occurs at the front of the vault in the wind direction.
- **Minimum Pressure (Suction):** Also increases in magnitude with the height-to-span ratio, mainly occurring at the center of the curved surface for ratios 0.4–0.6, and at the side flat surfaces for ratios 0.1–0.3.
- **Pressure Distribution:** For lower ratios (0.1–0.3), the front one-third of the vault is under positive pressure while the remainder experiences suction. For higher ratios (0.4–0.6), the front one-third remains under pressure, but the central curved region experiences stronger suction.
- **Optimal Ratio:** The vault with a height-to-span ratio of 0.1 shows the most balanced and favorable pressure distribution, with lower suction levels overall.

This trend shows that **increasing the height-to-span ratio amplifies both pressure and suction**, highlighting the sensitivity of taller vaults to wind loading.

3.2 Impact of Opening Dimensions on the Internal Pressure Coefficient Distribution of Barrel Vaults

Studies on the wind load acting on the outer surface of Vault showed that the Vault with a height-to-span ratio of 0.1 has the optimal ratio against wind flow. However, due to its very low height-to-span ratio, it is practically not used. Field studies indicated that the Vault with a height-to-span ratio of 0.5, because of its larger covered volume, is the most commonly used among Vault. Therefore, in this study, the effect of the opening dimensions on the flat surface of the Vault with a height-to-span ratio of 0.5 and a length-to-span ratio of one was investigated. To perform a comprehensive study, the ratio of the opening area to the flat surface area of the Vault on each side was selected as 0.1, 0.2, 0.3, 0.4, 0.5, 0.6, and 1. Also, the height-to-width

ratio of the openings was chosen as 1.75 and positioned at the center of the span. These dimensional ratios were chosen for two reasons:

First, the selected opening dimensions and their locations correspond to the doors of industrial sheds. Second, the only dimensional ratio that could remain constant on the openings with ratios from 0.1 to 0.6 on the flat surface of the Vault with a height-to-span ratio of 0.5 was in the range of 1.7 to 1.8, so 1.75 was selected.

The contour plots of the internal pressure coefficient variations for these Vaults are presented in Figures 11 to 60. For better comparison of these contours, their color scale ranges were standardized between -1.5 to 1 with steps of 0.1. The wind direction in all these figures is from right to left.

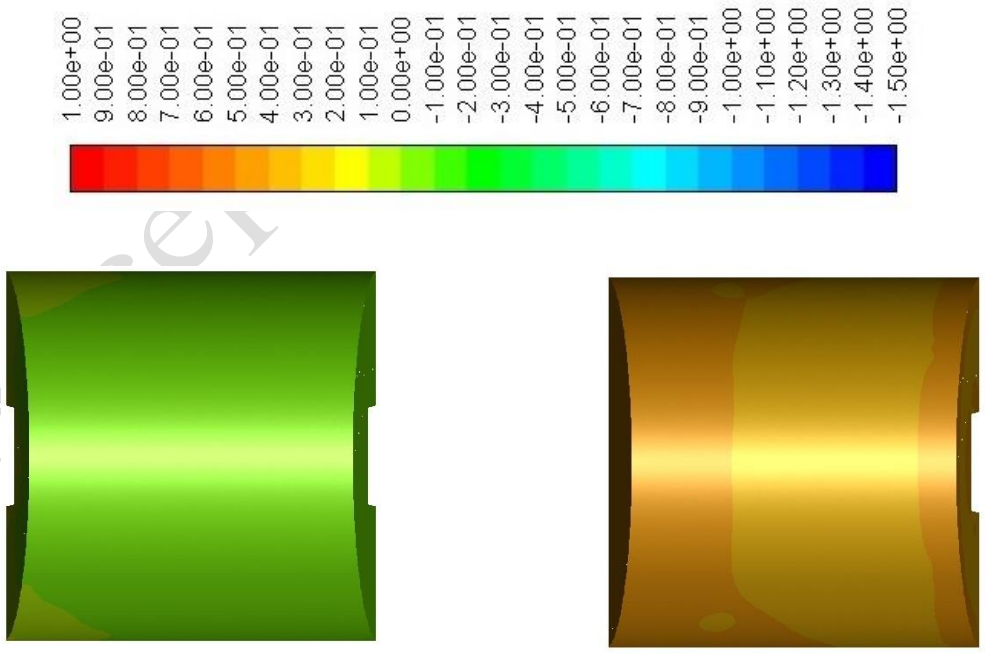

Fig 12. Contour of internal pressure coefficient distribution for the Vault with an inlet opening ratio of 0.1 and an outlet opening ratio of 0.1.

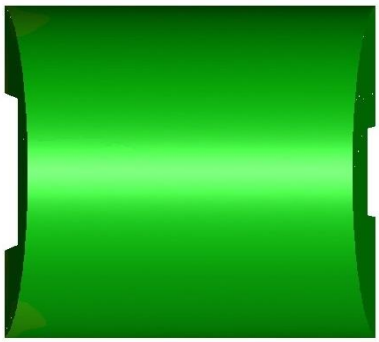

Fig. 14. Contour of internal pressure coefficient distribution for the Vault with an inlet opening ratio of 0.1 and an outlet opening ratio of 0.3.

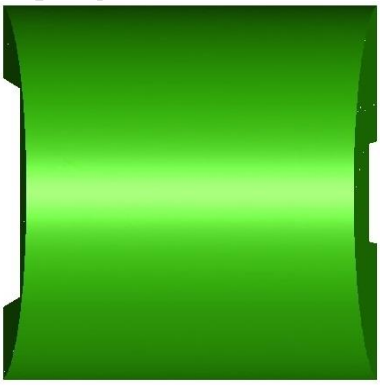

Fig. 11. Contour of internal pressure coefficient distribution for the Vault with an inlet opening ratio of 0.1 and an outlet opening ratio of 0.

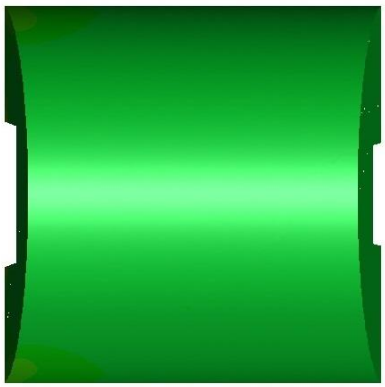

Fig. 13. Contour of internal pressure coefficient distribution for the Vault with an inlet opening ratio of 0.1 and an outlet opening ratio of 0.2.

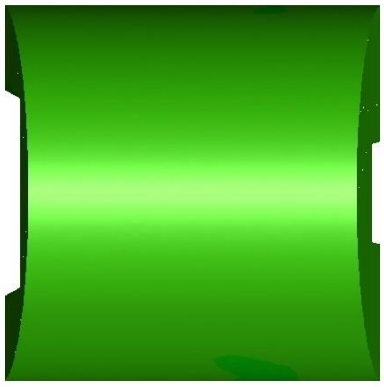

Fig. 16. Contour of internal pressure coefficient distribution for the Vault with an inlet opening ratio of 0.1 and an outlet opening ratio of 0.5.

Fig 15. Contour of internal pressure coefficient distribution for the Vault with an inlet opening ratio of 0.1 and an outlet opening ratio of 0.4.

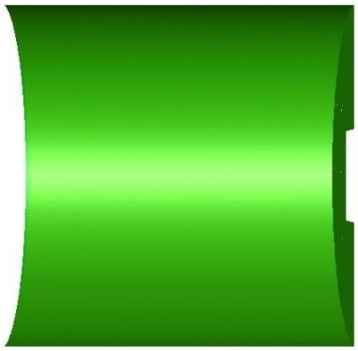

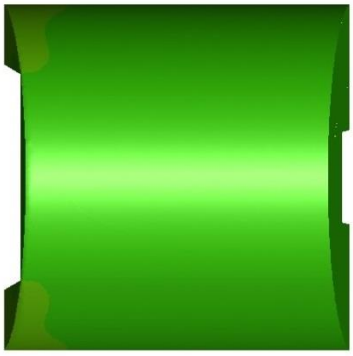

Fig. 18. Contour of internal pressure coefficient distribution for the Vault with an inlet opening ratio of 0.1 and an outlet opening ratio of 1.

Fig. 17. Contour of internal pressure coefficient distribution for the Vault with an inlet opening ratio of 0.1 and an outlet opening ratio of 0.6.

The internal pressure coefficient distribution for vaults with an inlet opening ratio of 0.1 and varying outlet opening ratios (0 to 1.0) is summarized in **Table 3**. As shown, when the outlet is closed (Figure 11), the vault is fully under positive pressure. Introducing an outlet (Figures 12–18) shifts the regime to suction. The suction magnitude increases with outlet ratios up to 0.3 (Figures 12–14), but for larger outlet ratios (Figures 15–18) the suction decreases slightly and stabilizes.

Table 3. Summary of internal pressure coefficient results for Figures 11–18

Figure	Inlet opening ratio	Outlet opening ratio	Cp range (min–max)	Overall regime	Key observation
Fig. 11	0.1	0	0.3 ~ 0.5	Positive pressure	Vault fully under pressure
Fig. 12	0.1	0.1	-0.1 ~ 0.1	Mostly suction, small end regions under low pressure	Suction begins with outlet
Fig. 13	0.1	0.2	-0.3 ~ -0.2	Suction	Stronger suction
Fig. 14	0.1	0.3	-0.3 ~ -0.2	Suction	Similar to 0.2, no major change
Fig. 15	0.1	0.4	-0.2 ~ -0.1	Suction	Suction decreases slightly
Fig. 16	0.1	0.5	-0.2 ~ -0.1	Suction	No significant change
Fig. 17	0.1	0.6	-0.2 ~ -0.1	Suction	Stable suction regime
Fig. 18	0.1	1.0	-0.2 ~ -0.1	Suction	Stable suction regime

Trend Summary for Figures 11 to 18:

- When the outlet opening ratio is 0 (Fig. 11), the entire vault is under positive internal pressure.
- Introducing a small outlet opening (0.1 in Fig. 12) initiates suction in most regions, while the end areas remain under low pressure.
- Increasing the outlet opening ratio to 0.2 and 0.3 (Figs. 13–14) intensifies suction over larger portions of the vault, though the change from 0.2 to 0.3 is not significant.
- Further increasing the outlet opening ratio to 0.4–1.0 (Figs. 15–18) slightly reduces suction, stabilizing the vault in a steady suction regime.
- Overall, increasing the outlet opening ratio shifts the internal pressure state from positive to suction, with major changes occurring up to a ratio of approximately 0.3, after which the internal pressure variations become limited.

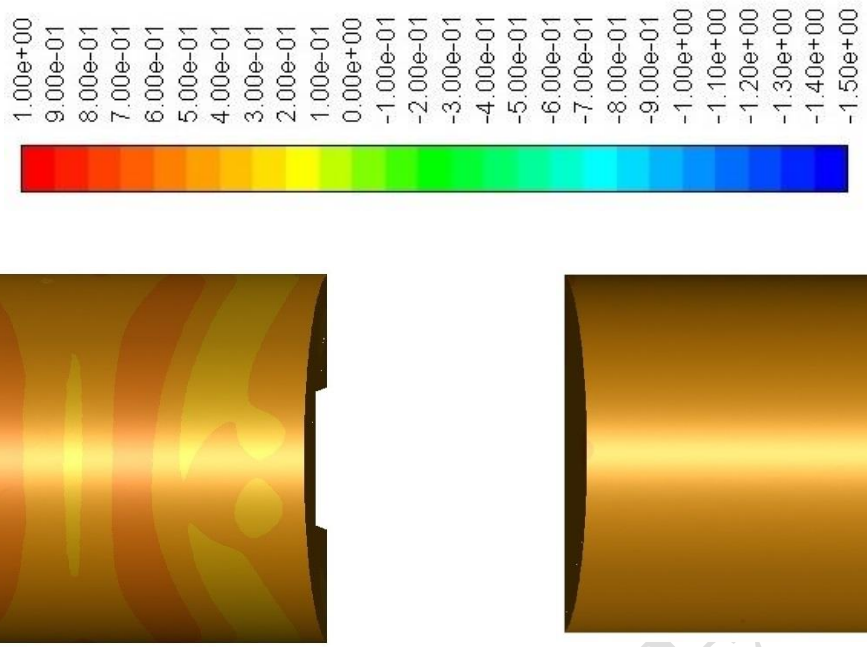

Fig. 20. Contour of internal pressure coefficient distribution of the Vault with an inlet opening ratio of 0.2 and an outlet opening ratio of 0.1.

Fig. 19. Contour of internal pressure coefficient distribution of the Vault with an inlet opening ratio of 0.2 and an outlet opening ratio of 0.

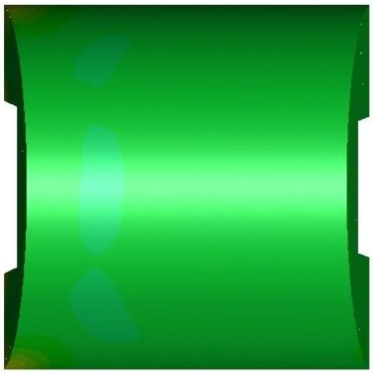

Fig. 22. Contour of internal pressure coefficient distribution of the Vault with an inlet opening ratio of 0.2 and an outlet opening ratio of 0.3.

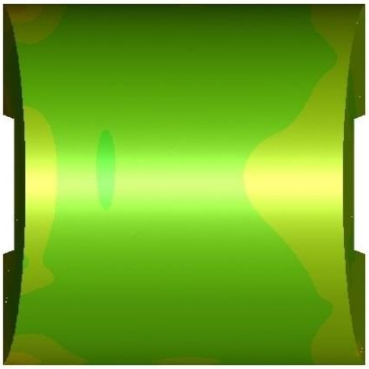

Fig. 21. Contour of internal pressure coefficient distribution of the Vault with an inlet opening ratio of 0.2 and an outlet opening ratio of 0.2.

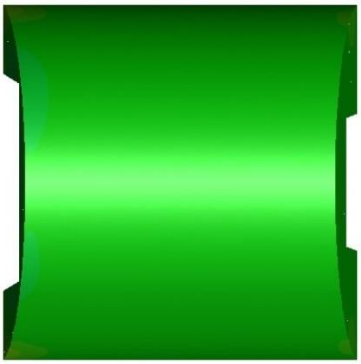

Fig. 24. Contour of internal pressure coefficient distribution of the Vault with an inlet opening ratio of 0.2 and an outlet opening ratio of 0.5.

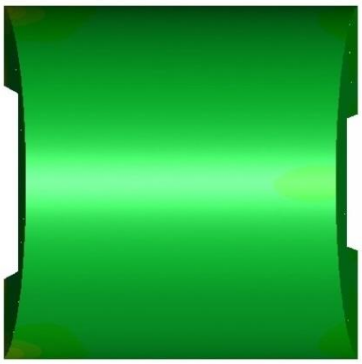

Fig. 23. Contour of internal pressure coefficient distribution of the Vault with an inlet opening ratio of 0.2 and an outlet opening ratio of 0.4.

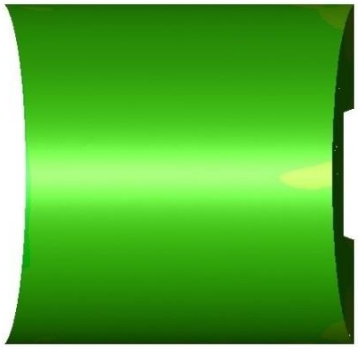

Fig. 26. Contour of internal pressure coefficient distribution of the Vault with an inlet opening ratio of 0.2 and an outlet opening ratio of 1.

Fig. 25.| Contour of internal pressure coefficient distribution of the Vault with an inlet opening ratio of 0.2 and an outlet opening ratio of 0.6.

Table 4 Summary of Results for Figures 19–26 (Inlet Opening = 0.2)

Figure	**Inlet Opening Ratio**	**Outlet Opening Ratio**	**Internal Pressure Coefficient Range**	**Pressure/Suction Condition**	**Key Observation**
19	0.2	0.0	0.4 → 0.5	Pressure (positive)	Higher internal pressure compared to Inlet=0.1, Outlet=0
20	0.2	0.1	0.3 → 0.6	Pressure (positive)	About 0.1 increase in pressure compared to Fig. 19
21	0.2	0.2	-0.1 → 0.1	Mixed (Pressure + Suction)	Edges under pressure, middle region under suction
22	0.2	0.3	-0.3 → -0.5	Suction (negative)	Entire vault under suction
23	0.2	0.4	-0.3 → -0.4	Suction (negative)	No significant change compared to Fig. 22
24	0.2	0.5	-0.3 → -0.4	Suction (negative)	Slight reduction in suction
25	0.2	0.6	-0.3 → -0.1	Suction (negative)	Further reduction in suction

26	0.2	1.0	-0.1 → -0.2	Weak suction (negative)	Suction weakens and range narrows

Trend Summary:

Outlet = 0: Positive internal pressure.

Outlet < Inlet (0.1–0.2): Mostly pressure, with partial suction in the middle.

Outlet ≥ Inlet (≥0.3): Suction dominates the entire structure.

Outlet > 0.4: Increasing outlet size only slightly reduces suction.

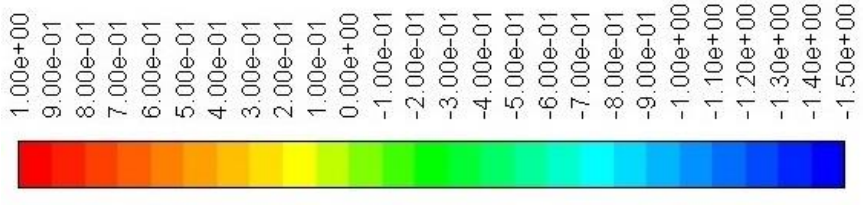

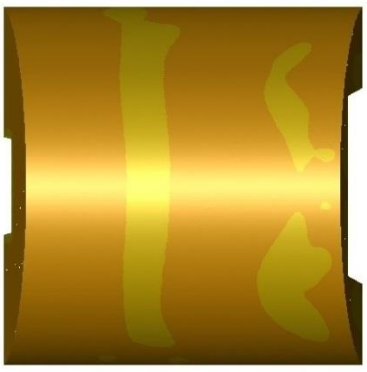

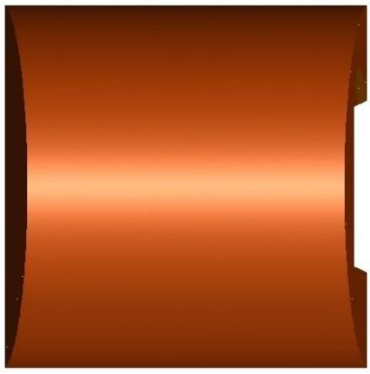

Fig. 28. Contour of internal pressure coefficient distribution of the Vault with an inlet opening ratio of 0.3 and an outlet opening ratio of 0.1.

Fig. 27. Contour of internal pressure coefficient distribution of the Vault with an inlet opening ratio of 0.3 and an outlet opening ratio of 0.

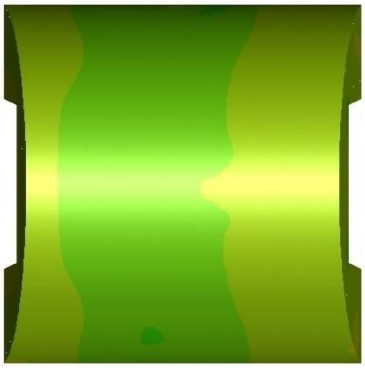

Fig. 30. Contour of internal pressure coefficient distribution in the Vault with an inlet opening ratio of 0.3 and an outlet opening ratio of 0.3.

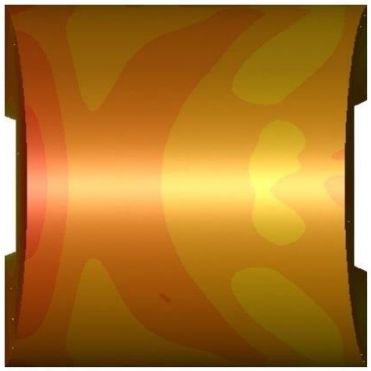

Fig. 29. Contour of internal pressure coefficient distribution of the Vault with an inlet opening ratio of 0.3 and an outlet opening ratio of 0.2.

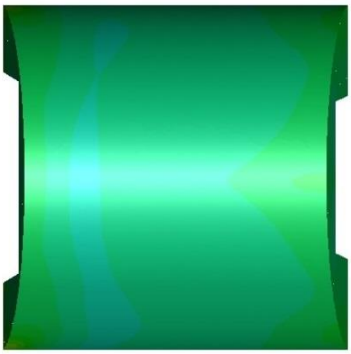

Fig. 32. Contour of internal pressure coefficient distribution in the Vault with an inlet opening ratio of 0.3 and an outlet opening ratio of 0.5.

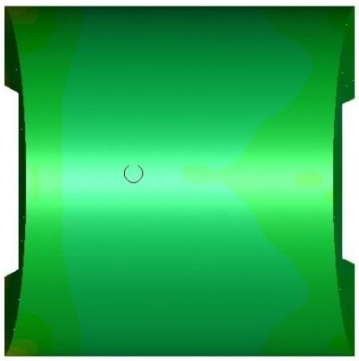

Fig. 31. Contour of internal pressure coefficient distribution in the Vault with an inlet opening ratio of 0.3 and an outlet opening ratio of 0.4.

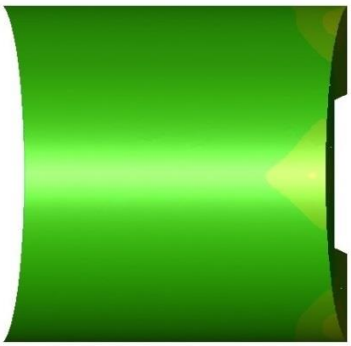

Fig. 34. Contour of internal pressure coefficient distribution in the Vault with an inlet opening ratio of 0.3 and an outlet opening ratio of 1.

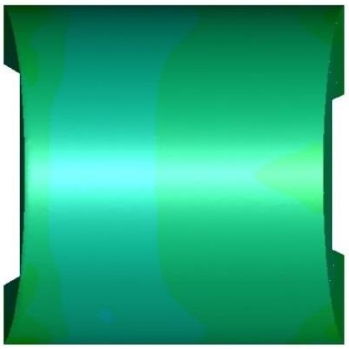

Fig. 33. Contour of internal pressure coefficient distribution in the Vault with an inlet opening ratio of 0.3 and an outlet opening ratio of 0.6.

Table 5: Variation of Internal Pressure Coefficient and Pressure Regime in Vaults with Inlet Opening Ratio of 0.3 for Different Outlet Opening Ratios (Figures 27–34)

Figure	**Inlet Opening Ratio**	**Outlet Opening Ratio**	**Min Internal Pressure Coefficient**	**Max Internal Pressure Coefficient**	**Pressure Regime**
27	0.3	0	0.4	0.5	Positive Pressure
28	0.3	0.1	0.3	0.5	Positive Pressure
29	0.3	0.2	0.3	0.8	Positive Pressure
30	0.3	0.3	-0.1	1	Mixed (Suction & Pressure)
31	0.3	0.4	-0.5	-0.3	Suction
32	0.3	0.5	-0.7	-0.4	Suction
33	0.3	0.6	-0.7	-0.4	Suction
34	0.3	1	-0.2	0	Suction

Trend Summary:

- When there is no outlet opening (Outlet Ratio = 0), the Vault experiences **positive internal pressure** across all points.

- Small outlet openings (0.1–0.2) maintain **mostly positive pressure**, but with slight local suction at some points.
- When the inlet and outlet opening ratios are equal (0.3/0.3), the Vault experiences a **mixed pressure regime**, with central regions under slight suction and edges under pressure.
- As the outlet opening ratio increases beyond the inlet opening (0.4–1), the Vault is predominantly under **suction**, with internal pressure coefficients decreasing as outlet size increases, except at full outlet opening (ratio = 1) where the suction slightly decreases.
- Increasing the outlet ratio by small increments (e.g., 0.3 → 0.4, 0.4 → 0.5) leads to noticeable increases in suction magnitude, but beyond 0.5, changes are minimal

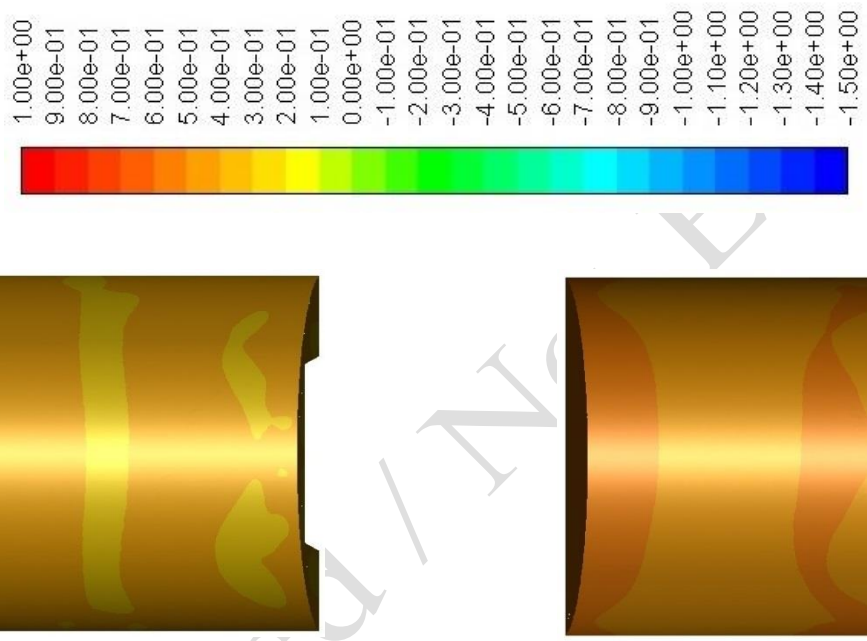

Fig. 36. Contour of internal pressure coefficient distribution in the barrel vault with an inlet opening ratio of 0.4 and an outlet opening ratio of 0.1.

Fig. 35. Contour of internal pressure coefficient distribution in the barrel vault with an inlet opening ratio of 0.4 and no outlet opening (0.0).

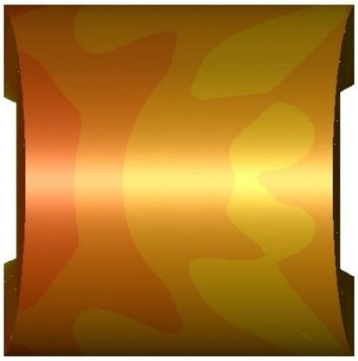

Fig. 38. Contour of internal pressure coefficient distribution in the barrel vault with an inlet opening ratio of 0.4 and an outlet opening ratio of 0.3.

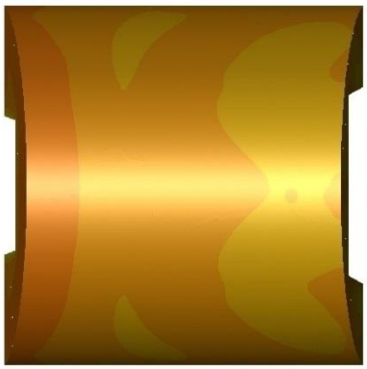

Fig. 37. Contour of internal pressure coefficient distribution in the barrel vault with an inlet opening ratio of 0.4 and an outlet opening ratio of 0.2.

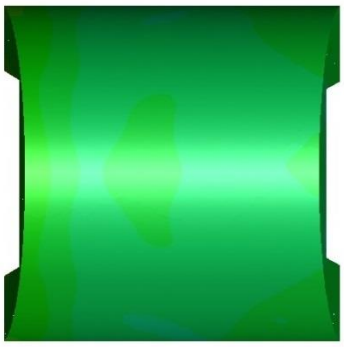

Fig. 40. Contour of internal pressure coefficient distribution in the barrel vault with an inlet opening ratio of 0.4 and an outlet opening ratio of 0.5.

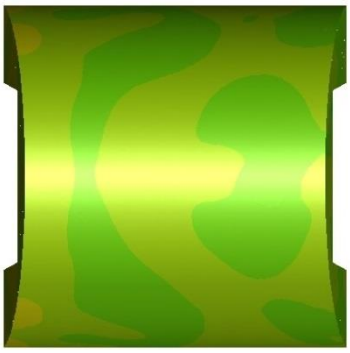

Fig. 39. Contour of internal pressure coefficient distribution in the barrel vault with an inlet opening ratio of 0.4 and an outlet opening ratio of 0.4.

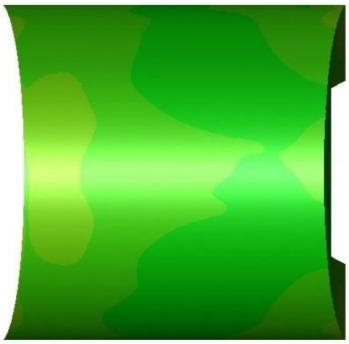

Fig. 42. Contour of internal pressure coefficient distribution in the barrel vault with an inlet opening ratio of 0.4 and an outlet opening ratio of 1.

Fig. 41. Contour of internal pressure coefficient distribution in the barrel vault with an inlet opening ratio of 0.4 and an outlet opening ratio of 0.6.

Table 6: Internal Pressure Coefficient Ranges and Pressure Regimes in Vaults with Inlet Opening Ratio of 0.4 for Different Outlet Opening Ratios (Figures 35–42)

Figure	Inlet Opening Ratio	Outlet Opening Ratio	Pressure Coefficient Range (Cp)	Pressure Regime
35	0.4	0	0.4 – 0.6	Positive
36	0.4	0.1	0.3 – 0.5	Positive
37	0.4	0.2	0.3 – 0.6	Positive
38	0.4	0.3	0.3 – 0.7	Positive
39	0.4	0.4	–0.1 – 0.1	Mixed
40	0.4	0.5	–0.3 – –0.5	Negative
41	0.4	0.6	–0.4 – –0.9	Negative
42	0.4	1	–0.3 – 0	Negative

Trend Summary (Figures 35–42, Inlet Opening Ratio = 0.4):

1. **Positive Pressure Dominance:**
    - When the outlet opening area is smaller than the inlet (outlet ratio 0–0.3), the vault experiences overall positive internal pressure. The Cp ranges gradually increase from 0.4–0.6 to 0.3–0.7 as the outlet ratio increases.
2. **Mixed Pressure Regime:**
    - When the outlet area equals the inlet (outlet ratio = 0.4), part of the vault is under suction while the other part remains under positive pressure, resulting in the lowest Cp values across the structure (–0.1 to 0.1).
3. **Negative Pressure Dominance:**

- When the outlet opening is larger than the inlet (outlet ratio 0.5–0.6), the vault experiences strong suction with Cp dropping to –0.4 to –0.9.
- Further increasing the outlet to 1 reduces the suction magnitude, bringing the Cp range to –0.3 to 0.

4. **Key Insight:**
   - Maintaining a larger inlet opening than outlet promotes positive internal pressure. Equal openings create mixed conditions with minimal Cp values. Larger outlet openings result in strong suction, but very large outlets (fully open) reduce the suction intensity.

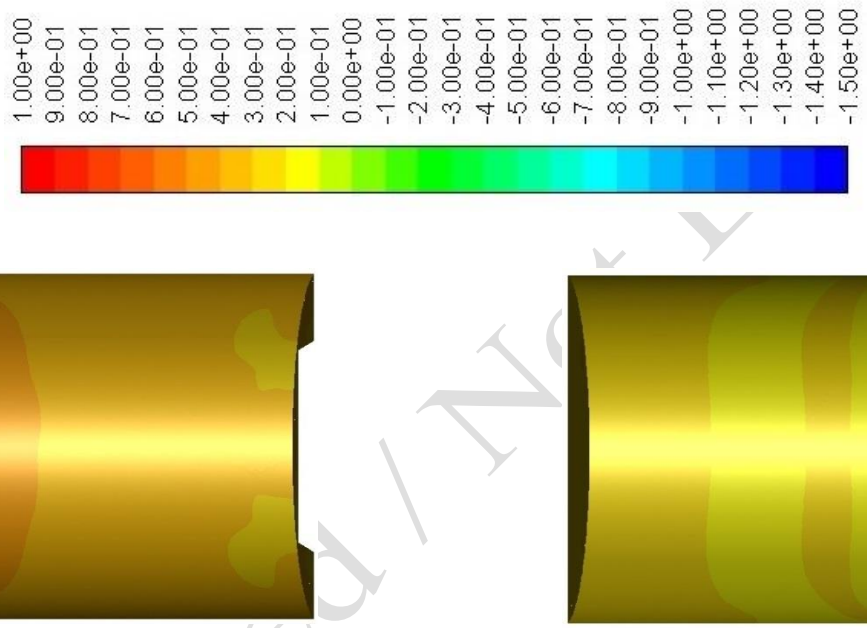

Fig. 44. Contour of internal pressure coefficient distribution for a barrel vault with an inlet opening ratio of 0.5 and an outlet opening ratio of 0.1.

Fig. 43. Contour of internal pressure coefficient distribution for a barrel vault with an inlet opening ratio of 0.5 and an outlet opening ratio of 0.

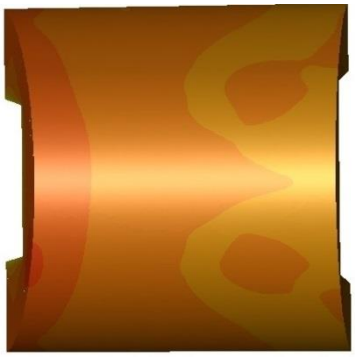

Fig. 46. Contour of internal pressure coefficient distribution for a barrel vault with an inlet opening ratio of 0.5 and an outlet opening ratio of 0.3.

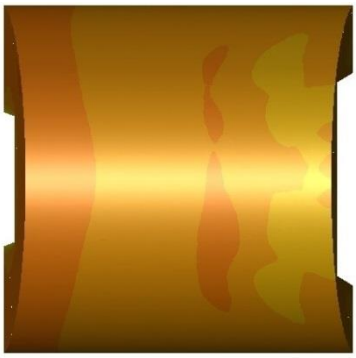

Fig. 45. Contour of internal pressure coefficient distribution for a barrel vault with an inlet opening ratio of 0.5 and an outlet opening ratio of 0.2.

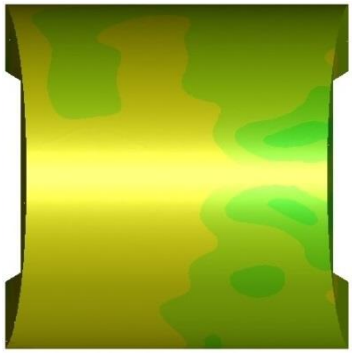

Fig. 48. Contour of internal pressure coefficient distribution for a barrel vault with an inlet opening ratio of 0.5 and an outlet opening ratio of 0.5.

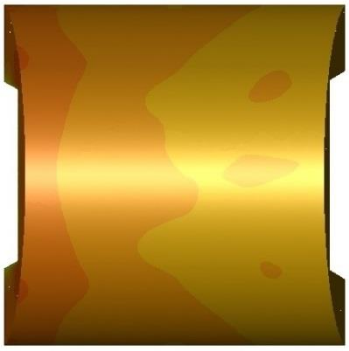

Fig. 47. Contour of internal pressure coefficient distribution for a barrel vault with an inlet opening ratio of 0.5 and an outlet opening ratio of 0.4.

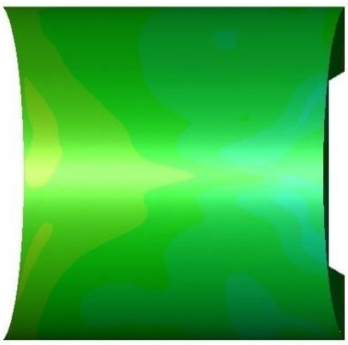

Fig. 50. Contour of internal pressure coefficient distribution for a barrel vault with an inlet opening ratio of 0.5 and an outlet opening ratio of 1.

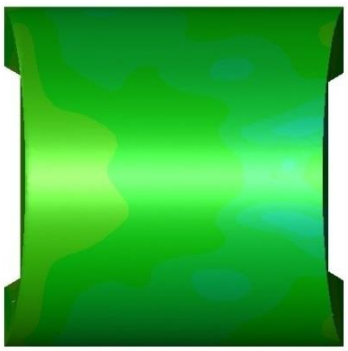

Fig. 49. Contour of internal pressure coefficient distribution for a barrel vault with an inlet opening ratio of 0.5 and an outlet opening ratio of 0.6.

Table 7 : Internal Pressure Coefficient Ranges for Vaults with Inlet Opening Ratio = 0.5 (Figures 43–50)

Figure	Inlet Opening Ratio	Outlet Opening Ratio	Cp Range	Pressure Regime
43	0.5	0	0.1 – 0.3	Positive
44	0.5	0.1	0.2 – 0.5	Positive
45	0.5	0.2	0.4 – 0.6	Positive
46	0.5	0.3	0.4 – 0.7	Positive
47	0.5	0.4	0.3 – 0.7	Mixed
48	0.5	0.5	–0.2 – 0.1	Mixed
49	0.5	0.6	–0.3 – –0.7	Negative
50	0.5	1	–0.5 – 0	Negative

Trend Summary (Figures 43–50, Inlet Opening Ratio = 0.5):

1. **Positive Pressure Dominance:**
    - When the outlet opening is smaller than the inlet (0–0.3), the vault experiences overall positive internal pressure.
2. **Mixed Pressure Regime:**
    - When the outlet equals the inlet (0.4–0.5), some regions are under pressure while others experience suction, producing the lowest Cp values.
3. **Negative Pressure Dominance:**

- When the outlet is larger than the inlet (0.6–1), the vault experiences suction, with Cp dropping to –0.7. For a fully open outlet (ratio = 1), the suction decreases slightly to a range of –0.5 to 0.

4. **Key Insight:**
   - Maintaining a larger inlet than outlet promotes positive internal pressure. Equal openings create mixed conditions, and larger outlet openings lead to significant suction, which slightly reduces when fully open.

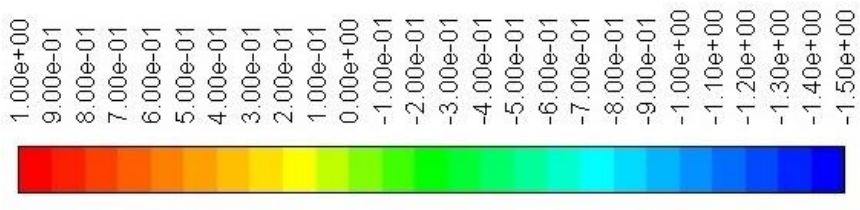

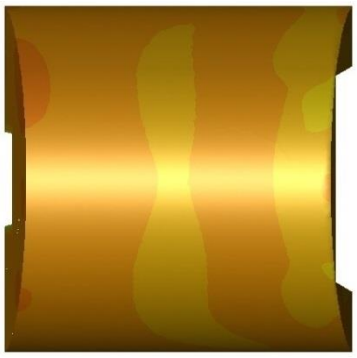

Fig. 52. Contour of internal pressure coefficient distribution of the vault with an inlet opening ratio of 0.6 and an outlet opening ratio of 0.1.

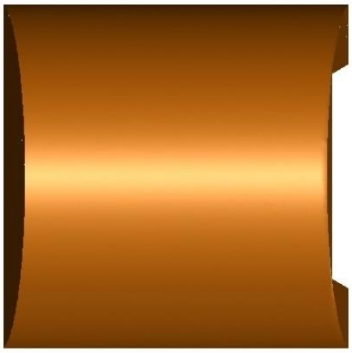

Fig. 51. Contour of internal pressure coefficient distribution of the vault with an inlet opening ratio of 0.6 and an outlet opening ratio of 0.

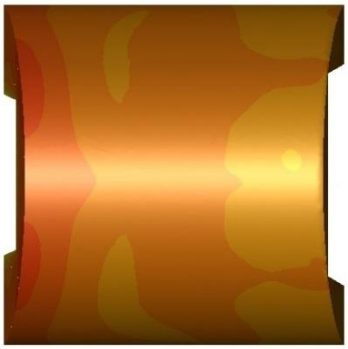

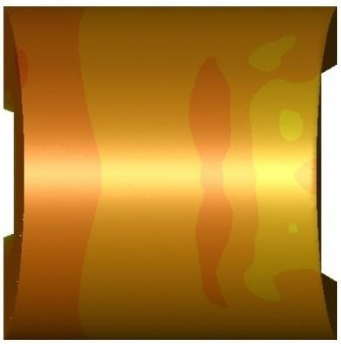

Fig. 54. Contour of internal pressure coefficient distribution of the vault with an inlet opening ratio of 0.6 and an outlet opening ratio of 0.3.

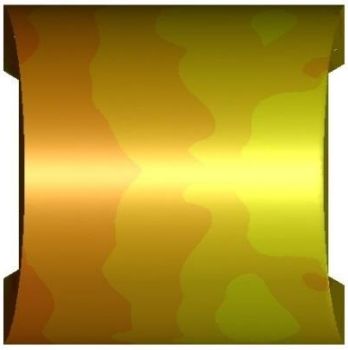

Fig. 56. Contour of internal pressure coefficient distribution of the vault with an inlet opening ratio of 0.6 and an outlet opening ratio of 0.5.

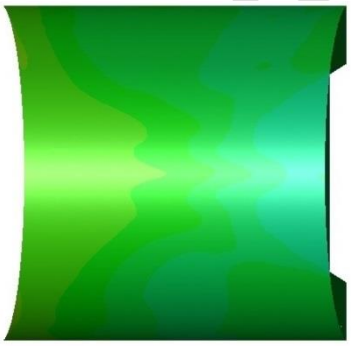

Fig. 58. Contour of internal pressure coefficient distribution of the vault with an

Fig. 53. Contour of internal pressure coefficient distribution of the vault with an inlet opening ratio of 0.6 and an outlet opening ratio of 0.2.

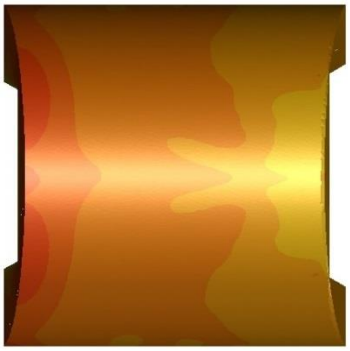

Fig. 55. Contour of internal pressure coefficient distribution of the vault with an inlet opening ratio of 0.6 and an outlet opening ratio of 0.4.

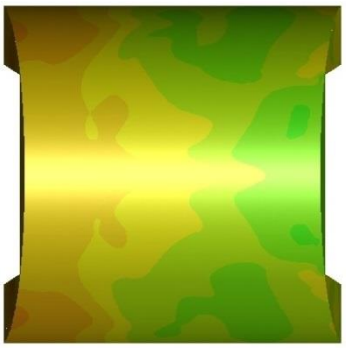

Fig. 57. Contour of internal pressure coefficient distribution of the vault with an

inlet opening ratio of 0.6 and an outlet opening ratio of 1.

inlet opening ratio of 0.6 and an outlet opening ratio of 0.6.

Table 8: Internal Pressure Coefficient Ranges for Vaults with Inlet Opening Ratio of 0.6 and Varying Outlet Opening Ratios (Figures 51–58)

Figure	Inlet Opening Ratio	Outlet Opening Ratio	Cpi Range	Pressure Regime
51	0.6	0	0.5 – 0.6	Positive
52	0.6	0.1	0.3 – 0.6	Positive
53	0.6	0.2	0.2 – 0.6	Positive
54	0.6	0.3	0.4 – 0.8	Positive
55	0.6	0.4	0.3 – 0.8	Mixed
56	0.6	0.5	0.1 – 0.6	Mixed
57	0.6	0.6	-0.1 – 0.4	Mixed/Suction
58	0.6	1	-0.2 – -0.7	Suction

Trend Summary:

- When the inlet opening area is larger than the outlet, the entire internal surface is under positive pressure.
- If the inlet and outlet areas are equal, part of the structure is under pressure and part under suction (mixed regime).
- When the outlet opening area exceeds the inlet area, the internal surface experiences suction, but the magnitude does not always increase with increasing outlet area.
- The optimal internal pressure distribution occurs when the inlet and outlet areas are equal, with the internal pressure coefficient ranging between -0.1 and 0.1 for vaults with inlet and outlet ratios from 0.1 to 0.5

A comparative plot of the maximum and minimum internal pressure coefficients (Max Cp and Min Cp) for different inlet and outlet opening ratios is presented in Figure 59. This figure highlights the variation of pressure regimes across the barrel vault roof under different scenarios.

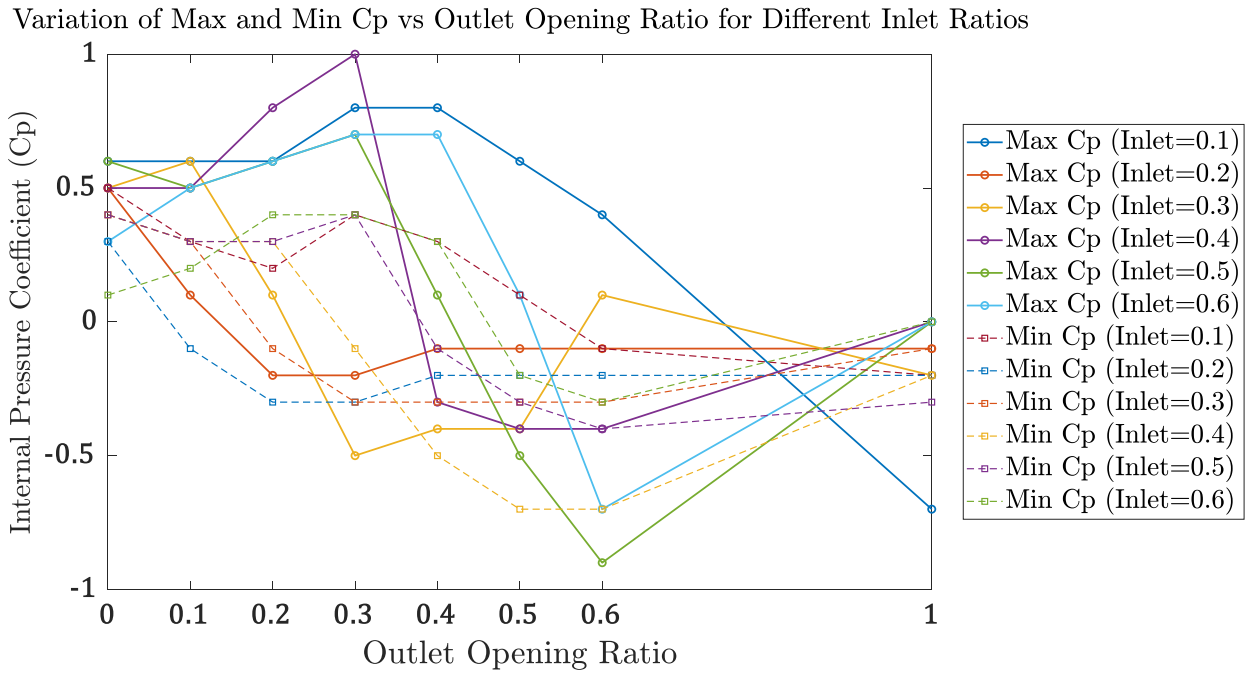

Figure 59. Variation of maximum and minimum internal pressure coefficients (Max Cp and Min Cp) with different inlet and outlet opening ratios in barrel vault structures.

4. Summary and Conclusion

This paper presents a comprehensive study on barrel vaults and the effect of openings on the distribution of internal pressure coefficients. The boundary layer flow over barrel vaults with different height-to-span ratios was investigated. The modeling results showed that the barrel vault with a height-to-span ratio of 0.1 represents the most optimal condition.

Quantitative evaluation of the vault models reveals that when the inlet opening area is larger than the outlet opening area, the entire internal surface of the structure is under pressure. When the inlet and outlet opening areas are equal, part of the structure experiences pressure while the other part experiences suction. Conversely, when the outlet opening area exceeds the inlet opening area, the entire internal surface is under suction. The optimal internal pressure distribution occurs when the inlet and outlet opening areas are equal, with the internal pressure

coefficient ranging between -0.1 and 0.1 for vaults having equal inlet and outlet opening ratios between 0.1 and 0.5.

The results indicated that when the inlet opening area is larger than the outlet opening area, the entire internal surface of the structure is under pressure; when the inlet and outlet opening areas are equal, part of the structure is under pressure and part under suction; and when the outlet opening area is larger than the inlet opening area, the entire internal surface is under suction.

The optimal internal pressure distribution occurs when the inlet and outlet opening areas are equal, where the internal pressure coefficient ranges between -0.1 and 0.1 for vaults with equal inlet and outlet opening ratios between 0.1 and 0.5.

The findings of this study have important engineering implications for the design of barrel vault roofs. Understanding the relationship between inlet and outlet opening areas allows engineers to optimize internal pressure distribution, enhancing structural safety and performance. For instance, ensuring that inlet and outlet openings are balanced can minimize areas under excessive suction or pressure, reducing the risk of structural failure and improving the efficiency of load-bearing elements. These insights can also guide practical design decisions and inform future updates to design codes for vaulted structures with openings.

While the present study provides comprehensive insights into the effects of opening dimensions and windward-to-leeward ratios on internal wind pressures in barrel vault roofs, certain limitations remain. Only a specific range of height-to-span ratios and opening

configurations were analyzed, and the simulations were conducted under idealized terrain and wind conditions. Future research could extend this work by considering a wider range of geometric parameters, more complex environmental conditions, and experimental validation to further enhance the reliability of predictions for practical applications.

The findings of this research provide practical guidance for engineers and can form a basis for more precise guidelines in building codes for estimating internal wind loads in structures with openings.

Acknowledgments

The authors would like to acknowledge the use of AI tools during the preparation of this manuscript to enhance its clarity, readability, coherence, and overall quality, ensuring that the presentation of ideas and results is clear and well-structured.

Notations

C_p = Pressure coefficient;

C_μ = Ground (or terrain) category coefficient;

E = Young's modulus;

E^K = Kinetic energy;

g_i = Gravitational acceleration components;

G = Shear modulus;

V_i = Velocity component in i direction;

U_{avg}= Average ratio of speed to velocity;

W^V = Viscous loss term;

ε = Strain;

ΔP = Pressure difference;

Φ = Viscous heat generation;

I = Turbulence intensity;

K = Thermal conductivity;

P = Flow Pressure;

Re = Reynolds number

R_i = Distributed resistance components;

T_i = Viscous loss terms components;

T_0 = Total temperature;

τ_{ij} = Stress tensor;

u_i = Orthogonal velocities;

μ = Dynamics viscosity;

μ_e = Effective viscosity;

λ = Second coefficient of viscosity;

σ = Stress;

ρ = Density

References

American Society of Civil Engineers (ASCE). (1998). Minimum design loads for buildings and other structures (ASCE 7-98). Reston, VA: ASCE. https://ascelibrary.org/doi/book/10.1061/9780784404454

ANSYS Inc. (2017). ANSYS Fluent theory guide, Release 18.2. Canonsburg, PA: ANSYS Inc.

Cheng, C. M., & Fu, C. L. (2000). "Characteristic of wind loads on a hemispherical dome in smooth flow and turbulent boundary layer flow." Journal of Wind Engineering and Industrial Aerodynamics, 44. https://doi.org/10.1016/j.jweia.2009.12.002

Cheon, D.-J., Kim, Y.-C., & Yoon, S.-W. (2024). "A proposal of wind pressure coefficients for structural frame design of dome roof structures with openings." Journal of the Architectural Institute of Korea, 40(6), 199–207. https://doi.org/10.5659/JAIK.2024.40.6.199

Ding, W., & Uematsu, Y. (2022). "Discussion of design wind loads on a vaulted free roof." Wind, 2(3), 479–494. https://doi.org/10.3390/wind2030026

Ding, W., Uematsu, Y., & Wen, L. (2023). "Fundamental characteristics of wind loading on vaulted-free roofs." Wind, 3(4), 394–417. https://doi.org/10.3390/wind3040023

Horr, A. M., Safi, M., & Alavinasab, S. A. (2003). "Computational wind tunnel analyses for large domes using CFD theory." International Journal of Space Structures, 18(2), 85–103. https://doi.org/10.1260/026635103769518206

Khosrowjerdi, S., & Sarkardeh, H. (2022). "Effect of wind load on combined arches in dome buildings." European Physical Journal Plus, 137, 227. https://doi.org/10.1140/epjp/s13360-022-02438-8

Khosrowjerdi, S., Sarkardeh, H., & Kioumarsi, M. (2021). "Effect of wind load on different heritage dome buildings." European Physical Journal Plus, 136, 133. https://doi.org/10.1140/epjp/s13360-021-02133-0

Lee, J. H., Kim, Y. C., Cheon, D. J., & Yoon, S. W. (2022). "Wind pressure characteristics of elliptical retractable dome roofs." Journal of Asian Architecture and Building Engineering, 21(4), 1561–1577. https://doi.org/10.1080/13467581.2021.1941996

Letchford, C. W., & Sarkar, P. P. (2000). "Mean and fluctuating wind loads on rough and smooth parabolic domes." Journal of Wind Engineering and Industrial Aerodynamics, 88. https://doi.org/10.1016/S0167-6105(00)00030-1

Li, M., Zhang, X., Bao, Y., Lin, J., Pei, C., Cheng, X., & Ma, C. (2025). "The influence of roof opening and closure on the overall wind pressure distribution of airport terminal roof."

Buildings, 15(5), 735. https://doi.org/10.3390/buildings15050735
Liu, W., Zhang, X., Chen, Y., & Wang, R. (2024). "Numerical analysis of roof wind pressure distribution in renovated historical buildings: Preventive protection measures to mitigate typhoon damage." Applied Sciences, 14(14), 6136. https://doi.org/10.3390/app14146136
Mahdi, M. T. (2004). "Performance of traditional arches, vaults and domes in the 2003 BAM earthquake." Asian Journal of Civil Engineering, 5(3–4), 209–221.
Pagnini, L., Torre, S., Freda, A., & Piccardo, G. (2022). "Wind pressure measurements on a vaulted canopy roof." Journal of Wind Engineering and Industrial Aerodynamics, 223, 104934. https://doi.org/10.1016/j.jweia.2023.105740
Rani, N., Pratap, A., & Ahuja, A. K. (2024). "Evaluation of wind pressure distribution on single and multi span cylindrical canopy roofs using wind tunnel testing." KSCE Journal of Civil Engineering, 28, 3344–3358. https://doi.org/10.1007/s12205-024-1013-8
Pratap, A., & Rani, N. (2025). A new parametric equation for wind pressure coefficient on low-rise mono-slope canopy roof building. KSCE Journal of Civil Engineering, 29(3), 100022. https://doi.org/10.1016/j.kscej.2024.100022
Reddy, J. N., & Gartling, D. K. (2000). The finite element method in heat transfer and fluid dynamics (2nd ed.). Boca Raton, FL: CRC Press. https://doi.org/10.1201/9781439882573
Sun, Y., Wu, Y., Qiu, Y., & Tamura, Y. (2015). "Effects of free-stream turbulence and Reynolds number on the aerodynamic characteristics of a semicylindrical roof." Journal of Structural Engineering, 141(9), 1–20. https://doi.org/10.1061/(ASCE)ST.1943-541X.0001209
Shukla, K. (2024). Effective location of shear walls in high-rise RCC buildings subjected to lateral loads. Civil Engineering Infrastructures Journal, 57(1), 103-117. 10.22059/ceij.2023.350020.1879
Uematsu, Y., Kuribara, O., Yamada, M., Sasaki, A., & Hongo, T. (2001). "Wind-induced dynamic behavior and its load estimation of a single layer lattice dome with a long span." Journal of Wind Engineering and Industrial Aerodynamics, 89. http://dx.doi.org/10.1016/S0167-6105(01)00125-8
Yao, J., Peng, M., Huang, J., Zhang, Q., & Zhou, Y. (2024). "Numerical simulation study on wind pressure coefficient of variable cross-section arched roof." Results in Engineering, 21, 101844. https://doi.org/10.1016/j.rineng.2024.101844